A pristine record of outer Solar System materials from asteroid Ryugu's returned sample

Journal Item

nature astronomy

ARTICLES

https://doi.org/10.1038/s41550-022-01745-5

Check for updates

OPEN

A pristine record of outer Solar System materials from asteroid Ryugu's returned sample

Motoo Ito[1]✉, Naotaka Tomioka[1], Masayuki Uesugi[2], Akira Yamaguchi[3,4], Naoki Shirai[5,32], Takuji Ohigashi[4,6,33], Ming-Chang Liu[7], Richard C. Greenwood[8], Makoto Kimura[3], Naoya Imae[3,4], Kentaro Uesugi[2], Aiko Nakato[9], Kasumi Yogata[9], Hayato Yuzawa[6], Yu Kodama[10,34], Akira Tsuchiyama[11,12,13], Masahiro Yasutake[2], Ross Findlay[8], Ian A. Franchi[8], James A. Malley[8], Kaitlyn A. McCain[7], Nozomi Matsuda[7], Kevin D. McKeegan[7], Kaori Hirahara[14], Akihisa Takeuchi[2], Shun Sekimoto[15], Ikuya Sakurai[16], Ikuo Okada[16], Yuzuru Karouji[17], Masahiko Arakawa[18], Atsushi Fujii[9], Masaki Fujimoto[9], Masahiko Hayakawa[9], Naoyuki Hirata[18], Naru Hirata[19], Rie Honda[20,35], Chikatoshi Honda[19], Satoshi Hosoda[9], Yu-ichi Iijima[38], Hitoshi Ikeda[9], Masateru Ishiguro[21], Yoshiaki Ishihara[17], Takahiro Iwata[9], Kosuke Kawahara[9], Shota Kikuchi[22], Kohei Kitazato[19], Koji Matsumoto[23], Moe Matsuoka[9], Tatsuhiro Michikami[24], Yuya Mimasu[9], Akira Miura[9], Osamu Mori[9], Tomokatsu Morota[25], Satoru Nakazawa[9], Noriyuki Namiki[23], Hirotomo Noda[23], Rina Noguchi[26], Naoko Ogawa[9], Kazunori Ogawa[9], Tatsuaki Okada[9], Chisato Okamoto[38], Go Ono[9], Masanobu Ozaki[4,9], Takanao Saiki[9], Naoya Sakatani[27], Hirotaka Sawada[9], Hiroki Senshu[22], Yuri Shimaki[9], Kei Shirai[9], Seiji Sugita[25], Yuto Takei[9], Hiroshi Takeuchi[9], Satoshi Tanaka[9], Eri Tatsumi[28], Fuyuto Terui[29], Ryudo Tsukizaki[9], Koji Wada[22], Manabu Yamada[22], Tetsuya Yamada[9], Yukio Yamamoto[9], Hajime Yano[9], Yasuhiro Yokota[9], Keisuke Yoshihara[9], Makoto Yoshikawa[9], Kent Yoshikawa[9], Ryota Fukai[9], Shizuho Furuya[9,25], Kentaro Hatakeda[10], Tasuku Hayashi[9], Yuya Hitomi[10], Kazuya Kumagai[10], Akiko Miyazaki[9], Masahiro Nishimura[9], Hiromichi Soejima[10], Ayako Iwamae[10,36], Daiki Yamamoto[9,30], Miwa Yoshitake[9,37], Toru Yada[9], Masanao Abe[9], Tomohiro Usui[9], Sei-ichiro Watanabe[31] and Yuichi Tsuda[4,9]

Volatile and organic-rich C-type asteroids may have been one of the main sources of Earth's water. Our best insight into their chemistry is currently provided by carbonaceous chondritic meteorites, but the meteorite record is biased: only the strongest types survive atmospheric entry and are then modified by interaction with the terrestrial environment. Here we present the results of a detailed bulk and microanalytical study of pristine Ryugu particles, brought to Earth by the Hayabusa2 spacecraft. Ryugu particles display a close compositional match with the chemically unfractionated, but aqueously altered, CI (Ivuna-type) chondrites, which are widely used as a proxy for the bulk Solar System composition. The sample shows an intricate spatial relationship between aliphatic-rich organics and phyllosilicates and indicates maximum temperatures of ~30 °C during aqueous alteration. We find that heavy hydrogen and nitrogen abundances are consistent with an outer Solar System origin. Ryugu particles are the most uncontaminated and unfractionated extraterrestrial materials studied so far, and provide the best available match to the bulk Solar System composition.

Between June 2018 and November 2019, the Japan Aerospace Exploration Agency (JAXA) Hayabusa2 spacecraft undertook extensive remote sensing investigations of asteroid Ryugu. Data from the Near-IR Spectrometer (NIRS3) on board Hayabusa2 indicated that Ryugu might be composed of material similar to thermally- and/or shock-metamorphosed carbonaceous chondrite meteorites[1]; the closest match being the CY (Yamato-type) chondrites[2]. The low albedo of Ryugu can be explained by the presence of abundant carbon-rich components, in combination with grain size, porosity and space-weathering effects[3]. The Hayabusa2 spacecraft conducted two touchdowns and sample collections on Ryugu. The first touchdown on 21 February 2019 obtained surface material that was stored in Chamber A of the return capsule, and the second, on 11 July 2019, collected material close to an artificial crater formed by

A full list of affiliations appears at the end of the paper.

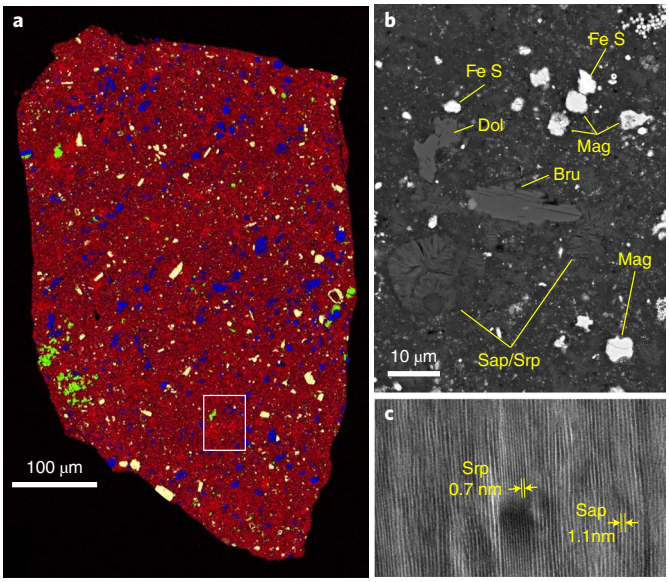

Fig. 1 | Thin-section images of Ryugu C0068. a, Combined X-ray map composed of Mg Kα (red), Ca Kα (green), Fe Kα (blue), and S Kα (yellow) of a dry-polished section of C0068. The section consists of phyllosilicate (red: ~88 vol%), carbonate (dolomite; light green: ~1.6 vol%), magnetite (blue: ~5.3 vol%) and sulfide (yellow: sulfide = ~2.5 vol%). **b**, Backscattered electron image of regions of outlined in **a**. Bru, breunnerite; Dol, dolomite; Fe S, Fe sulfide; Mag, magnetite; Sap, saponite; Srp, serpentine. **c**, High-resolution transmission electron microscopy (TEM) image of typical saponite–serpentine intergrowth area showing 0.7 nm and 1.1 nm lattice fringes of serpentine and saponite, respectively.

a small carry-on impactor. These samples were stored in Chamber C. Initial, non-destructive Phase 1 characterization of the particles in a dedicated, contamination-free and pure-nitrogen-filled chamber at the JAXA curation facility revealed that Ryugu particles were most similar to CI chondrites[4] and displayed 'a variety of alteration levels'[3]. The seemingly contradictory classifications of Ryugu, as similar to either CY or CI chondrites, can only be resolved by a detailed isotopic, elemental and mineralogical characterization of Ryugu particles. The results presented here provide a firm basis for determining which of these two preliminary interpretations of asteroid Ryugu's bulk composition is most likely.

Eight Ryugu particles (~60 mg in total), four from Chamber A and four from Chamber C, were allocated to the Phase 2 curation Kochi team. The principal goals of the research were to elucidate the nature, origin and evolutionary history of the asteroid Ryugu, and to document the similarities to, and differences from, other known extraterrestrial samples such as chondritic meteorites, interplanetary dust particles (IDPs) and returned cometary samples collected by the NASA Stardust mission.

Detailed mineralogical analysis of five Ryugu particles (A0029, A0037, C0009, C0014 and C0068) shows that they consist principally of fine- and coarse-grained phyllosilicates (~64–88 vol%; Fig. 1a,b, Supplementary Fig. 1 and Supplementary Table 1). Coarse-grained phyllosilicates as feathery aggregates (up to several tens of micrometres in size) occur in the fine-grained phyllosilicate-rich matrix (smaller than a few micrometres in size). The phyllosilicate grains are a serpentine–saponite intergrowth (Fig. 1c). A (Si + Al)–Mg–Fe plot further shows that bulk phyllosilicate matrices have intermediate compositions between serpentine and saponite (Fig. 2a,b). Carbonate minerals (~2–21 vol%), sulfide minerals (~2.4–5.5 vol%) and magnetite (~3.6–6.8 vol%) occur in the phyllosilicate matrix. One of the particles examined in this study (C0009) contains a small amount (~0.5 vol%) of anhydrous silicates (olivines and pyroxenes), which can potentially shed light on the original materials that constituted the protolith of Ryugu[5]. Such anhydrous silicates are rare in the Ryugu particles and have only been positively identified in particle C0009. Carbonates, appearing as fragments in the matrix (smaller than several hundred micrometres), are mainly dolomite, with minor Ca carbonate and breunnerite. Magnetite occurs as isolated grains, framboids, plaquettes or spherical aggregates. Sulfides are mostly pyrrhotite, showing irregular hexagonal prism/plate or lath morphologies. Abundant submicrometre-sized pentlandite occurs in the matrix or in association with pyrrhotite. Carbon-rich phases (<10 μm in size) occur ubiquitously in the phyllosilicate-rich matrix. Other accessory minerals are summarized in Supplementary Table 1. Mineral inventories identified by X-ray diffraction patterns of C0087 and a mixture of A0029 and A0037 are in good agreement with those identified in CI chondrites (Orgueil), but completely different from the CY and CM (Mighei-type) chondrites (Extended Data Fig. 1 and Supplementary Fig. 2). The bulk elemental abundances of Ryugu particles (A0098, C0068) are also consistent with those of CI chondrites[6] (Extended Data Fig. 2 and Supplementary Table 2). In contrast, CM chondrites are characterized by depletion of moderate- to highly volatile elements, particularly Mn and Zn, and have higher abundances of refractory elements[7]. Some elements show highly variable concentrations, which may be a reflection of inherent sample heterogeneity due to the small size of the individual particles and consequential sampling biases. All petrological, mineralogical and elemental characteristics indicate that the Ryugu particles are very similar to CI chondrites[8–10]. The remarkable exception is the absence of ferrihydrite and sulfate in the Ryugu particles, which indicates that these minerals in CI chondrites formed due to terrestrial weathering[11].

Bulk oxygen-isotope analysis by laser fluorination (Methods) was undertaken on a 1.83 mg sample of material extracted from particle C0014. For comparison purposes, we ran seven aliquots of Orgueil (CI) (total mass = 8.96 mg) and seven aliquots of Y-82162 (CY) (total mass = 5.11 mg) (Supplementary Table 3).

In Fig. 2d there is a clear separation in terms of both $\Delta^{17}O$ and $\delta^{18}O$ between the weighted averages for both Orgueil and the Ryugu particles compared with Y-82162. Ryugu particle C0014-4 has a higher $\Delta^{17}O$ than Orgueil, although there is overlap at the 2 s.d. level. The higher $\Delta^{17}O$ value of the Ryugu particle compared with Orgueil may reflect terrestrial contamination of the latter since its fall in 1864. Weathering in the terrestrial environment[11] would necessarily result in the incorporation of atmospheric oxygen and so pull the bulk analysis closer to the terrestrial fractionation line (TFL). This conclusion is consistent with the mineralogical evidence (discussed earlier) that Ryugu particles do not contain ferrihydrite or sulfate, whereas Orgueil does.

These results validate the link between Ryugu particles and CI chondrites based on the mineralogical evidence presented above, while seeming to exclude the possibility of a connection with the CY chondrites. The fact that the Ryugu particles are not related to the CY chondrites, which show clear mineralogical evidence for dehydration, is puzzling. Orbital observations of Ryugu seemed to indicate that it had experienced a dehydration and so was probably composed of CY material[2]. The reason for this apparent discrepancy remains unclear. Oxygen-isotope analysis of other Ryugu particles is presented in a companion paper[12]. However, the results from this extended dataset are also consistent with a link between Ryugu particles and CI chondrites.

Using coordinated microanalysis techniques (Supplementary Fig. 3), we studied the spatial distribution of organic carbon throughout the entire surface area of the C0068,25 focused-ion-beam (FIB) section (Fig. 3a–f). Carbon near-edge X-ray absorption fine-structure (NEXAFS) spectra in the C0068,25 section show a variety of functional groups—aromatic or C=C (285.2 eV), C=O

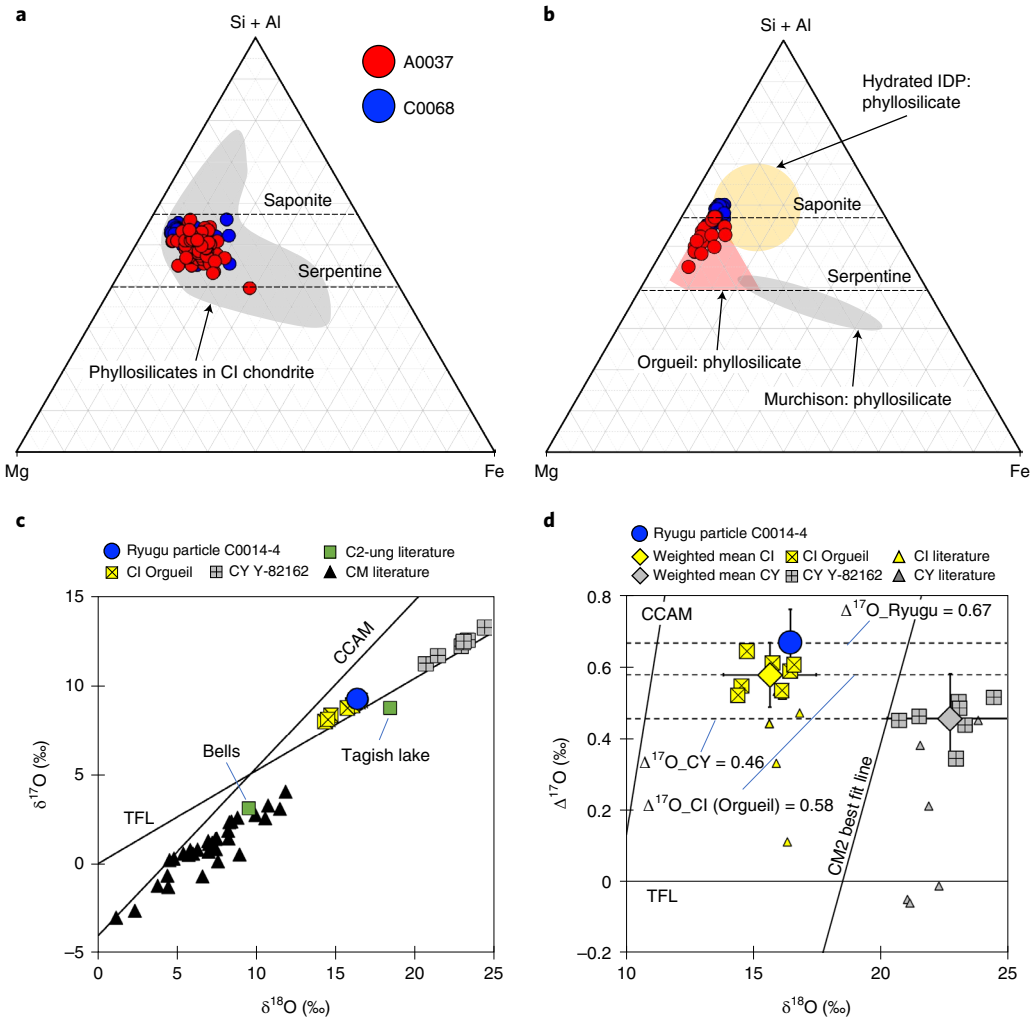

Fig. 2 | Major mineral components and bulk oxygen isotopic compositions of the Ryugu particles. Matrix and phyllosilicate compositions (at.%) from the Ryugu particles A0037 (filled red circles) and C0068 (filled blue circles) are shown in the ternary system (Si + Al)–Mg–Fe. **a**, The results of electron probe microanalysis (EPMA) are plotted with CI chondrites (Ivuna, Orgueil, Alais)[16] shown in the grey area for comparison. **b**, Scanning TEM (STEM)–energy-dispersive X-ray spectroscopy (EDS) analyses are shown for comparison with Orgueil[9] and Murchison[46] meteorites and hydrated IDPs[47]. Both fine- and coarse-grained phyllosilicates were analysed, avoiding small Fe sulfide grains. The dashed lines in **a** and **b** show the solid-solution lines for saponite and serpentine. Compositions highly enriched in Fe in **a** are probably caused by submicrometre-scale Fe sulfide grains within the phyllosilicate grains that could not be excluded in the spatial resolution of the EPMA analysis. The data points with higher Si contents than saponite in **b** could be caused by the presence of nanometre-scale Si-rich amorphous materials in the interstices of phyllosilicate layers. Numbers of analyses: $N = 69$ for A0037, $N = 68$ for C0068 for EPMA; $N = 19$ for A0037, $N = 27$ for C0068 for STEM–EDS. **c**, Three-oxygen-isotope diagram of Ryugu particle C0014-4 compared with CI (Orgueil), CY (Y-82162) and literature (CM, and C2-ung) chondrite values[41,48,49]. Data for Orgueil and Y-82162 meteorites were obtained in this study. CCAM, carbonaceous chondrite anhydrous mineral line; TFL, terrestrial fractionation line. **d**, $\Delta^{17}O$ versus $\delta^{18}O$ plot for Ryugu particle C0014-4, CI chondrites (Orgueil) and CY chondrites (Y-82162) (this study). $\Delta^{17}O$_Ryugu: $\Delta^{17}O$ value of C0014-1. $\Delta^{17}O$_Orgueil: average $\Delta^{17}O$ value of Orgueil. $\Delta^{17}O$_Y-82162: average $\Delta^{17}O$ value of Y-82162. CI and CY data from the literature[41,48,49] are also shown for comparison.

(286.5 eV), C–H (287.5 eV) and C(=O)O (288.8 eV)—without the graphene structure at 291.7 eV (Fig. 3a), implying low degrees of thermal alteration. The strong C–H peak (287.5 eV) of the organics in the C0068,25 section is distinct from the previously studied insoluble organic matter of carbonaceous chondrites[13] and shows more similarities with IDPs[14] and cometary particles obtained by the Stardust mission[15]. The strong C–H peak at 287.5 eV and the very weak aromatic or C=C peak at 285.2 eV imply that the organics are aliphatic-rich (Fig. 3a and Supplementary Fig. 3a). The aliphatic-rich organic areas are present locally within coarse-grained phyllosilicates, as well as within the regions with a poorly aromatic (or C=C) carbon structure (Fig. 3c,d). In contrast, the A0037,22 (Supplementary Fig. 3) section displays a lower abundance of aliphatic carbon-rich areas. The bulk mineralogy of these particles is carbonate-rich, similar to CI chondrites[16], and this is indicative of extensive parent body aqueous alteration (Supplementary Table 1). Oxidizing conditions would promote higher concentrations of carbonyl and carboxylic functional groups in the organic matter association with carbonates[17]. The submicrometre-scale distribution of organics with an aliphatic carbon structure may vary strongly depending on the distribution of coarse-grained phyllosilicates. A hint of aliphatic-bearing organics in association with phyllosilicate-OH has been reported in the Tagish Lake meteorite[18]. The coordinated microanalysis data suggest that aliphatic-rich organics may be widely distributed in C-type asteroids and exist in close association with phyllosilicates. This inference is consistent

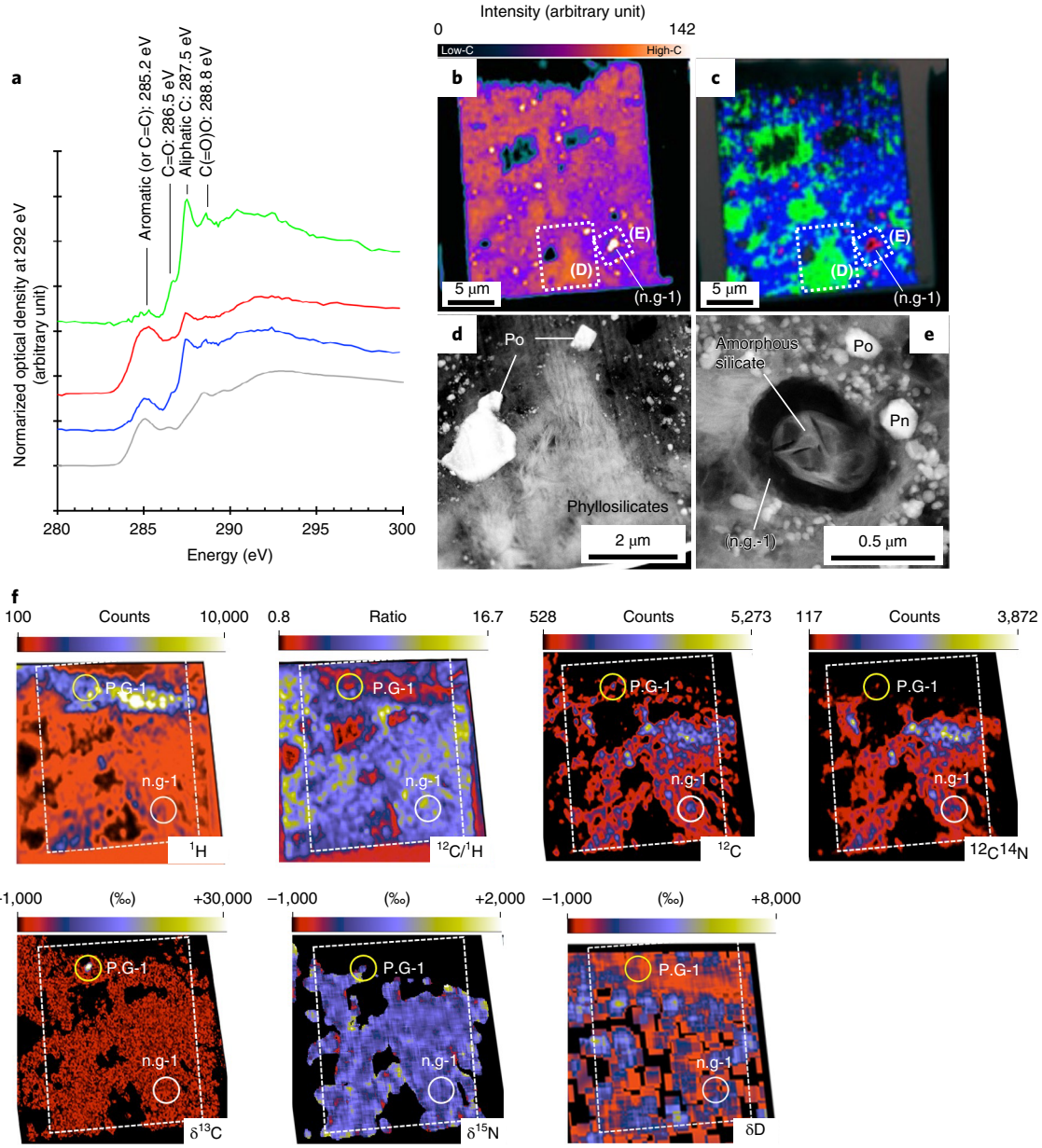

Fig. 3 | Analyses of a FIB section of C0068,25. a, Carbon NEXAFS spectra normalized to 292 eV of aromatic (C=C)-rich regions (red), aliphatic-rich regions (green) and matrix (blue). The grey line is a spectrum of Murchison insoluble organic matter[13] for comparison. a.u., arbitraty units. **b**, Scanning transmission X-ray microscope (STXM) carbon K-edge spectral image indicating that the section is dominated by carbon. **c**, Combined RGB map with aromatic-rich (C=C) areas (red), aliphatic-rich areas (green) and matrix (blue). **d**, Aliphatic-rich organics concentrated in coarse-grained phyllosilicates in an area enlarged from the white dashed boxes in **b** and **c**. **e**, Large nanoglobule (n.g-1) in area enlarged from the dashed white boxes in **b** and **c**. Po: pyrrhotite. Pn: pentlandite. **f**, Nanoscale secondary-ion mass spectrometry (NanoSIMS) elemental images of hydrogen (^{1}H), carbon (^{12}C) and nitrogen (^{12}C^{14}N), an elemental ratio image of ^{12}C/^{1}H, and isotope images of δD, δ^{13}C and δ^{15}N of the section. P.G-1: presolar graphite with extreme ^{13}C enrichment (Supplementary Table 4).

with a previous report of aliphatic/aromatic CH in the Ryugu particles demonstrated by MicrOmega, a hyperspectral microscope operating in the near-infrared range[3]. An important and as-yet-unresolved question is whether the unique nature of the aliphatic carbon-rich organics associated with coarse-grained phyllosilicates observed in this study is found only in the Ryugu asteroid.

A kinetic study of organic matter degradation in the Murchison meteorite[19] may provide important insight into the heterogeneous distribution of aliphatic-rich organics seen in the Ryugu particles. This study suggests that the aliphatic C–H bonds in organics survive at the maximum temperature of ~30°C on the parent body and/or will be lost depending on a time–temperature relationship (that is, 200 years at 100 °C and 100 million years at 0 °C). The initial distribution of aliphatic-rich organics in phyllosilicates could be preserved if the parent body was not heated beyond the time limit at a given temperature. However, aqueous alteration on the parent body might complicate this interpretation because carbonate-rich A0037 does not show any aliphatic carbon-rich regions associated with phyllosilicates. This low alteration temperature is broadly consistent with the occurrence of cubanite in Ryugu particles (Supplementary Table 1)[20].

A large nanoglobule was found in the C0068,25 section (n.g-1; Fig. 3a–c,e) showing highly aromatic (or C=C), moderately aliphatic and weakly C(=O)O and C=O spectra. The aliphatic carbon

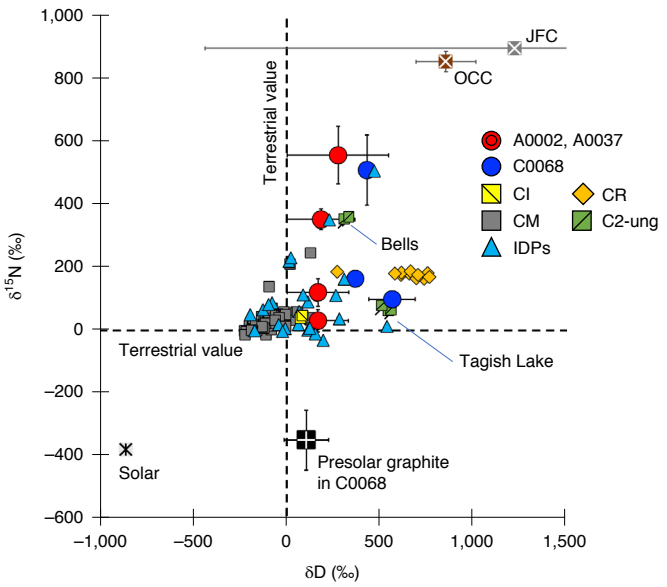

Fig. 4 | Light element isotopic compositions of the Ryugu particles A0002, A0037 and C0068. Comparison of the bulk H and N isotopic compositions of the Ryugu particles (red circles: A0002, A0037; blue circles: C0068) with solar values[27], the average Jupiter family (JFC[27]) and Oort Cloud (OCC[27]) comets, IDPs[28] and carbonaceous chondrites[27] (CI, CM, CR, C2-ung). The isotopic compositions are given in Supplementary Table 4. Dotted lines are the terrestrial isotopic values of H and N.

feature does not match that of the bulk insoluble organic matter and organic nanoglobules associated with chondritic meteorites (Fig. 3a)[17,21]. Raman and infrared spectroscopy analyses of nanoglobules in Tagish Lake show that they are composed of aliphatic and oxidized organic matter and disordered polycyclic aromatic organic matter, all of which are structurally complex[22,23]. The aliphatic carbon feature seen in n.g-1 may be an analytical artefact due to the surrounding matrix containing aliphatic-rich organics. Interestingly, n.g.-1 contains an embedded amorphous silicate (Fig. 3e), which is a texture that has not been reported for any extraterrestrial organics so far. The amorphous silicate could be a pristine component indigenous to n.g-1 or have originated from amorphization of hydrous/anhydrous silicate by ion- and/or electron-beam irradiation during analysis.

NanoSIMS ion images (Fig. 3f) of the C0068,25 section display homogeneous variation in $\delta^{13}C$ and $\delta^{15}N$, except for a presolar grain (P.G-1 in the $\delta^{13}C$ image in Fig. 3f) with a large ^{13}C enrichment of 30,811‰ (Supplementary Table 4). X-ray elemental and high-resolution TEM images of the grain show only the carbon concentration and the basal plane spacing of 0.3 nm, corresponding to graphite. It is worth noting that δD (841 ± 394‰) and $\delta^{15}N$ (169 ± 95‰) values of aliphatic-rich organics associated with coarse-grained phyllosilicates seem to be slightly higher than the average for the entire C regions (δD = 528 ± 139‰, $\delta^{15}N$ = 67 ± 15‰) in C0068,25 (Supplementary Table 4). This observation indicates that aliphatic-rich organics in coarse-grained phyllosilicates could be more primitive than the surrounding organics because the latter may have undergone isotopic exchange with surrounding water in the parent body[24]. Alternatively, these isotopic variations could also be linked to the initial formation process. In CI chondrites, the fine-grained phyllosilicates are interpreted to have formed via continued alteration of the initial coarse-grained clusters of anhydrous silicates[16]. Aliphatic-rich organics might have formed from precursor molecules either in the protoplanetary disk, or interstellar medium before the Solar System formed[24] and were then slightly modified during aqueous alteration in the Ryugu (grand)parent body. The size (<1.0 km) of Ryugu is too small to sufficiently maintain internal heat for aqueous alteration to form hydrous minerals[25]. Therefore, a precursor body to Ryugu of a few tens of kliometres in size may be required. Aliphatic-rich organics may have maintained their original isotopic ratios due to their association with coarse-grained phyllosilicates. However, the exact nature of the isotopically heavy carrier is still uncertain due to a complex fine-scale mixture of various components in these FIB sections. It could be either the aliphatic-rich organics or the surrounding coarse-grained phyllosilicates in Ryugu particles. Note that the organic matter is generally more enriched in D than the phyllosilicates in almost all carbonaceous chondrites, including CI chondrites, with the exception of the CM Paris meteorite[24,26].

A bulk δD and $\delta^{15}N$ plot of the A0002,23 and A0002,26, A0037,22 and A0037,23 and C0068,23, C0068,25 and C0068,26 FIB sections (a total of seven FIB sections from three Ryugu particles) obtained by NanoSIMS is shown in Fig. 4 (Supplementary Table 4) in comparison with other Solar System objects[27,28]. Variations in bulk δD and $\delta^{15}N$ in the A0002, A0037 and C0068 sections are compatible with those seen in IDPs but are higher than CM and CI chondrites (Fig. 4). Note that the range of δD values (−240 to 1,655‰) in Stardust cometary samples[29] is larger than that of Ryugu. The bulk δD and $\delta^{15}N$ of the Ryugu sections tend to be lighter than the average values of Jupiter family and Oort cloud comets (Fig. 4). The lower δD values for CI chondrites may reflect the influence of terrestrial contamination in these samples[30]. Given the similarities among Bells, Tagish Lake and IDPs, the large heterogeneity of the δD and $\delta^{15}N$ values in Ryugu particles may represent variations of the initial isotopic signatures of their organic and water components in the early Solar System[26]. The similar isotopic variations in δD and $\delta^{15}N$ in Ryugu particles and IDPs indicate that both could have formed from materials that came from the same source. IDPs are thought to have been derived from cometary sources[14]. Therefore, Ryugu could contain cometary-like and/or at least outer Solar System materials. However, it may be more complex than we claim here because of (1) a mixture of chondritic water and D-rich water on the parent body[31] and (2) the D/H ratio of comets depending on cometary activities[32]. However, the causes of the hydrogen and nitrogen isotopic heterogeneities observed in the Ryugu particles are not yet fully understood, due in part to the limited numbers of analyses available thus far. The results from hydrogen and nitrogen isotopic systems still raise the possibility that Ryugu contains a substantial portion of outer Solar System-derived materials and so could show some similarities with comets. The Ryugu sections show no obvious correlation between $\delta^{13}C$ and $\delta^{15}N$ (Supplementary Table 4).

The delivery of volatiles (that is, organics and water) to the Earth is still a subject of notable debate[26,27,33]. The submicrometre-scale organics associated with coarse-grained phyllosilicates in Ryugu particles, identified in this study, probably represent one important source of volatiles. Organics incorporated into coarse-grained phyllosilicates seem to be better protected from degradation[16,34] and breakdown[35] than those within fine-grained matrix. The heavier hydrogen isotopic composition of the particles means that they are unlikely to be the only source of volatiles delivered to the early Earth. They may have been mixed with components with lighter hydrogen isotopic compositions, as recently proposed by the hypothesis of solar-wind-derived water in silicates[36].

In this study we demonstrate that CI meteorites, despite their geochemical importance as proxies of the bulk Solar System composition[6,10], are terrestrially contaminated samples. We also provide direct evidence of an interaction between aliphatic-rich organics and adjacent hydrous minerals and show that Ryugu could contain outer Solar System-derived materials[37]. The findings of this study clearly demonstrate the importance of direct sampling of primitive asteroids and the need to transport returned samples in totally

inert and sterile conditions. The evidence presented here shows that Ryugu particles are undoubtedly among the most uncontaminated Solar System materials available for laboratory study and ongoing investigations of these precious samples will certainly expand our understanding of early Solar System processes. Ryugu particles are the best proxy we have for the bulk composition of the Solar System.

Methods

Designs of analyses of Ryugu particles. To determine the complex microtexture and chemical characteristics of the sample at submicrometre scales, we conducted coordinated microanalysis utilizing synchrotron radiation-based computed tomography (SR-XCT) and SR-X-ray diffractometry (XRD)-CT, FIB–STXM-NEXAFS–NanoSIMS–TEM analysis without degradation, contamination due to the terrestrial atmosphere and small particles or mechanical sample damage. In parallel, we carried out systematic bulk analysis with scanning electron microscopy (SEM)-EDS, EPMA, XRD, instrumental neutron activation analysis (INAA) and a laser fluorination oxygen-isotope facility. The analytical procedure is shown in Supplementary Fig. 3, and each analysis is described in the following sections.

Sample transportation and handling processes. The Ryugu asteroid particles were recovered from the Hayabusa2 re-entry capsule and transported to the JAXA Curation Facility at Sagamihara, Japan, without terrestrial atmospheric contamination[4]. After initial and non-destructive characterizations at the JAXA Curation Facility, an airtight facility-to-facility transfer container and a sample capsule pack (made of sapphire glass and stainless steel with 10 or 15 mm diameter depending on sample size) were used to avoid chemical reactions with the surrounding environment and/or terrestrial contaminants (for example, water vapour, hydrocarbons, atmospheric gases and small particles) and cross-contamination between samples during sample preparation and transportation among institutes and universities[38]. To avoid degradation and contamination due to interaction with the terrestrial atmosphere (water vapour and oxygen gas), all sample preparations (including chipping by a tantalum chisel, and cutting by a counter-balanced diamond wire saw (Meiwa Fosis Corporation DWS 3400) and epoxy mount preparation) were conducted in a glove box in an atmosphere of pure, dry N_2 (Dew point: −80 to −60 °C, O_2 ~50–100 ppm). All items used here were cleaned by a combination of ultrapure water and ethanol under ultrasonication with different frequencies.

We studied meteorite collections (CI: Orgueil, CM2.4: Yamato (Y)-791198, CY: Y-82162, and CY: Y 980115) of the Antarctic Meteorite Research Center at the National Institute of Polar Research (NIPR) in this study.

For the transfers between instruments for SR-XCT, NanoSIMS, STXM–NEXAFS and TEM analyses we used the universal holders for ultrathin film samples described in previous studies[38].

SR-XCT analysis. The SR-XCT analyses for Ryugu samples were performed with the integrated CT system at BL20XU/SPring-8. The integrated CT system consists of different measurement modes: the wide-field and low-resolution (WL) mode for capturing the entire structure of the sample, the narrow-field and high-resolution (NH) mode for precise measurement of the region of interest and the XRD mode to acquire the diffraction pattern of the bulk volume of the sample and perform XRD-CT to acquire 2D mineral phase maps of horizontal planes in the sample. Note that all measurements could be done without removing the sample holder from the mount using the integrated system, and therefore accurate measurements for CT and XRD-CT were possible. The X-ray detector for the WL mode (BM AA40P; Hamamatsu Photonics) was equipped with a complementary metal oxide semiconductor (CMOS) camera that had 4,608 × 4,608 pixels (C14120-20P; Hamamatsu Photonics), a scintillator consisting of a 10-μm-thick lutetium aluminium garnet ($Lu_3Al_5O_{12}$:Ce) single crystal and relay lenses. The pixel size of the WL mode was approximately 0.848 μm. Thus, the field of view (FOV) of the WL mode was ~6 mm with the offset CT scan mode. The X-ray detector for the NH mode (BM AA50; Hamamatsu Photonics) was equipped with a scintillator consisting of gadolinium aluminium gallium garnet ($Gd_3Al_2Ga_3O_{12}$) that was 20 μm thick, a CMOS camera that had 2,048 × 2,048 pixels (C11440-22CU; Hamamatsu Photonics) and a ×20 lens. The pixel size of the NH mode was ~0.25 μm and the FOV was ~0.5 mm. The detector for XRD mode (BM AA60; Hamamatsu Photonics) was equipped with a scintillator consisting of a P43 (Gd_2O_2S:Tb) powder screen that was 50 μm thick, a CMOS camera that had 2,304 × 2,304 pixels (C15440-20UP; Hamamatsu Photonics) and relay lenses. The effective pixel size of the detector was 19.05 μm and the FOV was 43.9 mm^2. To increase the FOV, we applied the offset CT procedure in the WL mode. Transmitted light images for CT reconstruction were composed by combining images of 180° to 360° that horizontally reflected around the rotation axis, with the images from 0° to 180°.

For the XRD mode, an X-ray beam was focused by a Fresnel zone plate. With this mode, the detector was located 110 mm behind the sample, with a beam stop 3 mm in front of the detector. Diffraction images of 2θ ranging from 1.43° to 18.00° (lattice spacing $d = 16.6–1.32$ Å) were acquired with an X-ray beam spot focusing on the bottom of the FOV of the detector. Samples were vertically translated with a certain interval, and a half-rotated for each vertical scan step. Diffraction of mineral grains in a horizontal plane can be obtained if the mineral grains meet the Bragg condition in the 180° rotation. Diffraction images were then integrated into one image for each vertical scan step[39]. The SR-XRD-CT analytical conditions were almost the same as for the SR-XRD analyses. For the XRD-CT mode, the detector was located 69 mm behind the sample. Diffraction images of 2θ ranging from 1.2° to 17.68° ($d = 19.73–1.35$ Å) were acquired with both an X-ray beam and a beam stop that were placed on a straight line to the centre of the FOV of the detector. The sample was scanned horizontally with 180° rotation of the sample. The SR-XRD-CT image was reconstructed using the peak intensity of minerals as the pixel value. Samples were typically scanned with 500 to 1,000 steps for a horizontal scan.

The X-ray energy was fixed to 30 keV for all experiments because it is the lower limit for X-ray penetration of meteorites that are ~6 mm in diameter[40]. The number of images acquired for all CT measurements during the 180° rotation was 1,800 (3,600 for the offset CT procedure), and the exposure time for images was 100 ms for the WL mode, 300 ms for the NH mode, 500 ms for XRD and 50 ms for XRD-CT. The typical scanning time for one sample was ~10 min in the WL mode, ~15 min in the NH mode, ~ 3 h for XRD, and 8 h for SR-XRD-CT.

CT images were reconstructed by a convolution-backprojection method and normalized for linear attenuation coefficients of 0 to 80 cm^{-1}. Slice software was applied for the analysis of 3D data, and muXRD software was used for the analysis of XRD data.

Optical, SEM–EDS and EPMA analyses. The epoxy-mounted Ryugu particles (A0029, A0037, C0009, C0014 and C0068) were polished on a surface in a stepwise manner down to the level of a 0.5 μm diamond lapping film (3M) under dry conditions avoiding elution of any materials from the surface during polishing. A polished surface of each sample was examined first by an optical microscope, and then by a JEOL JSM-7100F SEM equipped with an energy-dispersive spectrometer (AZtec energy) to obtain an overview of the mineralogy and textures of the samples by backscattered electron (BSE) images and qualitative elemental maps at NIPR. Major and minor elemental abundance analysis of each sample were conducted with an electron probe microanalyser (EPMA, JEOL JXA-8200). Phyllosilicate and carbonate grains were analysed with a current of 5 nA, and sulfide, magnetite, olivine and pyroxene with a current of 30 nA using natural and synthetic standards at 15 keV. Modal abundances were calculated from elemental maps and BSE images by utilizing the ImageJ 1.53 software with a proper threshold arbitrarily set for each mineral.

High-precision oxygen isotopic analysis. Oxygen isotopic analysis was undertaken at the Open University (Milton Keynes, UK) using an infrared laser-assisted fluorination system[41]. The Hayabusa2 samples were transported to the Open University in nitrogen-filled facility-to-facility transfer container[38].

Sample loading was undertaken in a nitrogen glove box with monitored oxygen levels below 0.1%. A new Ni sample holder was fabricated for the Hayabusa2 analysis work that consisted of just two sample wells (2.5 mm diameter, 5 mm depth); one for the Hayabusa2 particle and the other for the internal obsidian standard. During analysis, the sample well containing the Hayabusa2 material was overlain by an ~1-mm-thick, 3-mm-diameter internal BaF_2 window to retain the sample during laser reactions. The flow of BrF_5 to the sample was maintained by gas mixing channels cut into the Ni sample holder. The sample chamber configuration was also modified so that it could be removed from the fluorination line under vacuum and then opened within the nitrogen-filled glove box. The two-part chamber was made vacuum tight using a compression seal with a copper gasket and an EVAC quick-release CeFIX chain clamp[38]. The 3-mm-thick BaF_2 window at the top of the chamber allowed simultaneous viewing and laser heating of samples. Following sample loading, the chamber was then reclamped and reattached to the fluorination line. Before analysis the sample chamber was heated overnight under vacuum to a temperature of about 95 °C to remove any adsorbed moisture. Following overnight heating, the chamber was allowed to cool to room temperature and then the section that had been exposed to the atmosphere during the sample transfer process was purged using three aliquots of BrF_5 to remove any moisture. These procedures ensured that the Hayabusa2 samples were never exposed to the atmosphere or contaminated with moisture from those parts of the fluorination line that had been brought up to atmosphere during the sample loading procedure.

Ryugu particle C0014-4 and the Orgueil (CI) samples were run in modified 'single shot' mode[42], whereas analyses of Y-82162 (CY) were run in a single tray with multiple sample wells[41]. Owing to their anhydrous composition, it was not necessary to use the single-shot technique for the CY chondrites. Sample heating in the presence of BrF_5 was carried out using a Photon Machines Inc. 50 W infrared CO_2 laser (10.6 μm) mounted on an $X–Y–Z$ gantry. The progress of the reaction was monitored by means of an integrated video system. After fluorination, the released O_2 was purified by passing it through two cryogenic nitrogen traps and over a bed of heated KBr to remove any excess fluorine. The isotopic composition of the purified oxygen gas was analysed using a Thermo Fisher MAT 253 dual-inlet mass spectrometer with a mass resolving power of approximately 200.

In some cases the amount of O_2 gas liberated during sample reaction was less than 140 μg, the approximate limit for using the bellows facility on the MAT 253 mass spectrometer. In these cases, analysis was undertaken using the microvolume.

Following analysis of the Hayabusa2 particle, the internal obsidian standard was fluorinated, and its oxygen-isotope composition determined.

The NF^+ fragment ion of NF_3^+ can cause interference with the mass 33 beam ($^{16}O^{17}O$). To eliminate this potential problem, most samples were treated using a cryogenic separation procedure. This was either done in the forward sense before analysis on the MAT 253 or as a second analysis with the already analysed gas pulled back onto a dedicated molecular sieve and then rerun after cryogenic separation. Cryogenic separation involved taking the gas onto the molecular sieve at liquid nitrogen temperature and then releasing it to the main molecular sieve at a temperature of −130°C. Extensive tests have shown that NF^+ is retained on the first molecular sieve and that no substantial fractionation results from the use of this technique.

The overall system precision in bellows mode, as defined by replicate analyses of our internal obsidian standard[43], was: ±0.053‰ for $\delta^{17}O$; ±0.095‰ for $\delta^{18}O$; ±0.018‰ for $\Delta^{17}O$ (2 s.d.). Oxygen isotopic analyses are reported in standard δ notation, where $\delta^{18}O$ has been calculated as:

$$\delta^{18}O = \left[\left(^{18}O/^{16}O\right)_{\text{sample}} / \left(^{18}O/^{16}O\right)_{\text{VSMOW}} - 1\right] 1,000$$

and similarly for $\delta^{17}O$ using the $^{17}O/^{16}O$ ratio. VSMOW is the international standard Vienna Standard Mean Ocean Water. $\Delta^{17}O$, which represents the deviation from the terrestrial fractionation line, has been calculated as: $\Delta^{17}O = \delta^{17}O - 0.52 \times \delta^{18}O$. A blank correction has been applied to all the data presented in Supplementary Table 3.

Sample preparation using a FIB. Approximately 150- to 200-nm-thick sections were extracted from Ryugu particles using a Hitachi High Tech SMI4050 FIB instrument at the Kochi Institute for Core Sample Research, JAMSTEC. Note that all FIB sections were extracted from unprocessed broken pieces of original particles just after removal from facility-to-facility transfer containers filled with N_2 gas. The pieces were not measured by SR-CT and were handled with minimal exposure to the terrestrial atmosphere to avoid potential damage and contamination that could influence the carbon K-edge spectra. After deposition of tungsten protection layers, regions of interest (up to 25 × 25 μm²) were cut out and thinned using a Ga^+ ion beam at an accelerating voltage of 30 kV and then finalized at 5 kV and a probe current of 40 pA to minimize damage to surface layers. The ultrathin sections were subsequently mounted on scaled-up Cu grids (Kochi grids)[39] using a micromanipulator equipped with the FIB.

Elemental abundance measured by INAA. Ryugu particles A0098 (1.6303 mg) and C0068 (0.6483 mg) were doubly sealed in cleaned and high-purity polyethylene sheets in a pure N_2-filled glove box at SPring-8 without any interaction with the terrestrial atmosphere. Sample preparation of JB-1 (a geological standard rock sample issued by the Geological Survey of Japan) was carried out at Tokyo Metropolitan University.

INAA was performed at the Institute for Integrated Radiation and Nuclear Science, Kyoto University. Samples were irradiated two times with different irradiation periods chosen according to the half-lives of the nuclides used for elemental quantification. First, samples were irradiated for 30 s in pneumatic irradiation tube no. 3 with thermal and fast neutron fluxes of 4.6×10^{12} and 9.6×10^{11} cm^{-2} s^{-1}, respectively, to determine Mg, Al, Ca, Ti, V and Mn abundances. Chemical reagents such as MgO (99.99% purity; Soekawa Chemical), Al (99.9% purity; Soekawa Chemical) and Si metals (99.999% purity; FUJIFILM Wako Pure Chemical) were also irradiated to correct for interfering nuclear reactions such as (n,p). Sodium chloride (99.99% purity; MANAC) was also irradiated with the samples to correct for neutron flux variations.

After neutron irradiation, the outer polyethylene sheet was replaced with a new sheet and gamma rays emitted from the samples and reference standards were immediately measured using Ge detectors. The same samples were re-irradiated for 4 h in pneumatic irradiation tube no. 2 with thermal and fast neutron fluxes of 5.6×10^{12} and 1.2×10^{12} cm^{-2} s^{-1}, respectively, to determine Na, K, Ca, Sc, Cr, Fe, Co, Ni, Zn, Ga, As, Se, Sb, Os, Ir and Au abundances. Reference samples for Ga, As, Se, Sb, Os, Ir and Au were prepared by dropping a proper amount (10 to 50 μg) of concentration-known standard solutions of these elements onto the two sheets of filter paper, which were then irradiated with the samples. Gamma-ray counting was carried out at the Institute for Integrated Radiation and Nuclear Science, Kyoto University and RI Research Center, Tokyo Metropolitan University. The analytical procedure and reference materials for elemental quantification by INAA were the same as those described in our previous work[44].

Bulk mineralogy determined using XRD. An X-ray diffractometer (Rigaku SmartLab) was used to collect the diffraction patterns of Ryugu samples A0029 (<1 mg), A0037 (≪1 mg) and C0087 (<1 mg) at NIPR. All of the samples were ground to fine powders using a sapphire glass plate on a silicon non-reflection plate, and then homogeneously distributed onto the silicon non-reflection plate without any fluid (water or alcohol). The measurement conditions were as follows: Cu Kα X-rays were produced at 40 kV tube voltage and 40 mA tube current; the length of the limiting slit was 10 mm, the divergence angle was (1/6)°, the in-plane rotation speed was 20 r.p.m., the 2θ range (two-fold Bragg angle) was 3–100°, and it took ~28 h for each analysis. Bragg Brentano optics were used. The detector was a one-dimensional silicon semiconductor detector (D/teX Ultra 250). Cu Kβ X-rays were removed using a Ni filter. The peaks were identified by a comparison with the measured data using the available samples, synthesized Mg-saponite (JCSS-3501, Kunimine Industries CO. Ltd), serpentine (antigorite, Miyazu, Nichika) and pyrrhotite (monoclinic 4C, Chihuahua, Mexico) and using the powder diffraction file data from International Center for Diffraction Data, dolomite (PDF 01-071-1662) and magnetite (PDF 00-019-0629). The diffraction data for Ryugu were also compared with data for hydrously altered carbonaceous chondrites, Orgueil CI, Y-791198 CM2.4 and Y 980115 CY (heating stage III, 500–750 °C). The comparison showed similarities with Orgueil but not with Y-791198 and Y 980115.

Carbon functional groups identified using STXM–NEXAFS. The carbon K-edge NEXAFS spectra of ultrathin section samples made by FIB were measured using the STXM beam line, BL4U, at the UVSOR Synchrotron Facility, Institute for Molecular Science (Okazaki, Japan). The beam spot size focused with Fresnel zone-plate optics was about 50 nm. The energy step size was 0.1 eV in the fine-structure portions of the near-edge region (283.6–292.0 eV), and 0.5 eV in the pre-edge and post-edge regions (280.0–283.5 eV and 292.5–300.0 eV). The acquisition time per image pixel for each energy step was set to 2 ms. Helium gas at a pressure of ~20 mbar was backfilled with the STXM analysis chamber after evacuation. This helps to minimize the thermal drift of X-ray optics-related apparatus in the chamber and the sample holder, and to reduce sample damage and/or oxidation. The carbon K-edge NEXAFS spectra were obtained from stack data using the aXis2000 software and the in-house customized software for STXM data reduction. Note that an in-house, custom built sample transfer vessel and a glove box were used to avoid oxidization and contamination on the sample.

Hydrogen, carbon, and nitrogen isotopic imaging analysis using NanoSIMS. The hydrogen, carbon and nitrogen isotopic compositions of the Ryugu FIB sections were analysed using isotopic imaging with the JAMSTEC NanoSIMS 50L after STXM–NEXAFS analysis. A focused primary Cs^+ beam of approximately ~2 pA was used for carbon, and nitrogen isotopic analyses, and approximately ~13 pA was used for hydrogen isotopic analyses, rastered over approximately 24 × 24 μm² to 30 × 30 μm² areas on the samples. Each analysis was initiated after stabilization of the secondary-ion-beam intensity following 3 min of pre-sputtering with a relatively strong primary-ion-beam current. For carbon and nitrogen isotopic analysis, images of $^{12}C^-$, $^{13}C^-$, $^{16}O^-$, $^{12}C^{14}N^-$ and $^{12}C^{15}N^-$ were acquired simultaneously by multidetection with seven electron multipliers at a mass resolving power of approximately 9,000, which was sufficient to separate all relevant isobaric interferences (that is, $^{12}C^1H$ on ^{13}C and $^{13}C^{14}N$ on $^{12}C^{15}N$). For hydrogen isotopic analysis, images of $^1H^-$, $^2D^-$ and $^{12}C^-$ were acquired using three electron multipliers in multidetection at a mass resolving power of approximately 3,000. Each analysis consisted of 30 scanned images of the same area, with individual images consisting of 256 × 256 pixels for the carbon and nitrogen isotopic analyses and 128 × 128 pixels for the hydrogen isotopic analysis. The dwell times were 3,000 μs per pixel for the carbon and nitrogen isotopic analyses and 5,000 μ per pixel for the hydrogen isotopic analysis. We used 1-hydroxybenzotriazole hydrate as the hydrogen, carbon and nitrogen isotopic standards to correct for instrumental mass fractionation[45].

For silicon isotopic compositions of the presolar graphite in the C0068-25 FIB section, we acquired secondary-ion images of $^{12}C^-$, $^{13}C^-$, $^{16}O^-$, $^{28}Si^-$, $^{29}Si^-$ and $^{30}Si^-$ simultaneously by multidetection with six electron electron multipliers at a mass resolving power of approximately 9,000. These images consist of 256 × 256 pixels with a dwell time of 3,000 μs per pixel. We used a silicon wafer as the hydrogen, carbon and silicon isotopic standard to correct for instrumental mass fractionation.

The isotopic images were processed using the software NASA JSC imaging software for NanoSIMS[45]. Data were corrected for electron multiplier dead time (44 ns), and the quasi-simultaneous arrival effect. Different scans of each image were aligned to correct image drift during acquisition. Final isotopic images were generated by adding the secondary ions of each image from each pixel over the scans.

Micrometre- to submicrometre-scale mineralogical observations using TEM. After STXM–NEXAFS and NanoSIMS analysis, the same FIB sections were studied using a transmission electron microscope (JEOL JEM-ARM200F) operated at an accelerating voltage of 200 kV at Kochi, JAMSTEC. Microtextural observations were performed by bright-field TEM and high-angle annular dark-field scanning TEM imaging. Mineral phases were identified using selected-area electron diffraction and lattice-fringe imaging, and chemical analyses using EDS with a 100 mm² silicon drift detector and JEOL Analysis Station 4.30 software. For quantitative analyses, the intensities of the characteristic X-rays of each element were measured using a fixed acquisition time of 30 s, a beam scan area of ~100 × 100 nm² and a beam current of 50 pA in scanning TEM mode. The (Si + Al)–Mg–Fe ratios of phyllosilicates were determined using experimental thickness-corrected k factors obtained from a natural pyrope-almandine garnet standard.

Data availability

All images and analysis data used in this study are available at the JAXA Data Archives and Transmission System (DARTS) https://www.darts.isas.jaxa.jp/curation/hayabusa2. Source data are provided with this paper.

Code availability

Please add the details of the custom software and whether/where it is available here.

Received: 18 January 2022; Accepted: 23 June 2022;
Published online: 15 August 2022

References

1. Kitazato, K. et al. Surface composition of asteroid 162173 Ryugu as observed by the Hayabusa2 NIRS3 instrument. *Science* **364**, 272–275 (2019).
2. King, A. J. et al. The Yamato-type (CY) carbonaceous chondrite group: analogues for the surface of asteroid Ryugu? *Geochemistry* **79**, 125531 (2019).
3. Pilorget, C. et al. First compositional analysis of Ryugu samples by the MicrOmega hyperspectral microscope. *Nat. Astron.* **6**, 221–225 (2021).
4. Yada, T. et al. Preliminary analysis of the Hyabusa2 samples returned from C-type asteroid Ryugu. *Nat. Astron.* **6**, 214–220 (2021).
5. Liu, M-C. et al. Incorporation of 16O-rich anhydrous silicates in the protolith of highly hydrated asteroid Ryugu. *Nat. Astron.* (in the press).
6. Lodders, K. Relative atomic solar system abundances, mass fractions, and atomic masses of the elements and their isotopes, composition of the solar photosphere, and compositions of the major chondritic meteorite groups. *Space Sci. Rev.* **217**, 44 (2021).
7. Wasson, J. T. & Kallemeyn, G. W. Compositions of chondrites. *Phil. Trans. R. Soc. Lond. A* **325**, 535–544 (1988).
8. King, A. J. et al. Terrestrial modification of the Ivuna meteorite and a reassessment of the chemical composition of the CI type specimen. *Geochim. Cosmochim. Acta* **268**, 73–89 (2020).
9. Tomeoka, K. & Buseck, P. R. Matrix mineralogy of the Orgueil CI carbonaceous chondrite. *Geochim. Cosmochim. Acta* **52**, 1627–1640 (1988).
10. Barrat, J. A. et al. Geochemistry of CI chondrites: major and trace elements, and Cu and Zn Isotopes. *Geochim. Cosmochim. Acta* **83**, 79–92 (2012).
11. Gounelle, M. & Zolensky, M. E. A terrestrial origin for sulfate veins in CI1 chondrites. *Meteorit. Planet. Sci.* **36**, 1321–1329 (2001).
12. Greenwood, R. C. et al. Oxygen isotope evidence from asteroid Ryugu for early water delivery to Earth by CI chondrites. *Nat. Astron.* (in the press).
13. Cody, G. D. et al. Organic thermometry for chondritic parent bodies. *Earth Planet. Sci. Lett.* **272**, 446–455 (2008).
14. Keller, L. P. et al. The nature of molecular cloud material in interplanetary dust. *Geochim. Cosmochim. Acta* **68**, 2577–2589 (2004).
15. Sandford, S. A. et al. Organics captured from Comet 81P/Wild 2 by the Stardust spacecraft. *Science* **314**, 1720–1724 (2006).
16. Morlok, A. et al. Brecciation and chemical heterogeneities of CI chondrites. *Geochim. Cosmochim. Acta* **70**, 5371–5394 (2006).
17. Alexander, C. M. O. D. et al. Elemental, isotopic, and structural changes in Tagish Lake insoluble organic matter produced by parent body processes. *Meteorit. Planet. Sci.* **49**, 503–525 (2014).
18. Yesiltas, M. & Kebukawa, Y. Associations of organic matter with minerals in Tagish Lake meteorite via high spatial resolution synchrotron-based FTIR microspectroscopy. *Meteorit. Planet. Sci.* **51**, 584–595 (2016).
19. Kebukawa, Y. et al. Kinetics of organic matter degradation in the Murchison meteorite for the evaluation of parent-body temperature history. *Meteorit. Planet. Sci.* **45**, 99–113 (2010).
20. Berger, E. L. et al. Heterogeneous histories of Ni-bearing pyrrhotite and pentlandite grains in the CI chondrites Orgueil and Alais. *Meteorit. Planet. Sci.* **51**, 1813–1829 (2016).
21. De Gregorio, B. T. et al. Isotopic and chemical variation of organic nanoglobules in primitive meteorites. *Meteorit. Planet. Sci.* **48**, 904–928 (2013).
22. Garvie, L. A. J. & Buseck, P. R. Prebiotic carbon in clays from Orgueil and Ivuna (CI), and Tagish Lake (C2 ungrouped) meteorites. *Meteorit. Planet. Sci.* **42**, 2111–2117 (2007).
23. De Gregorio, B. T. et al. Isotopic anomalies in organic nanoglobules from comet 81P/Wild 2: comparison to Murchison nanoglobules and isotopic anomalies induced in terrestrial organics by electron irradiation. *Geochim. Cosmochim. Acta* **74**, 4454–4470 (2010).
24. Alexander, C. M. O. D. et al. The origin and evolution of chondrites recorded in the elemental and isotopic compositions of their macromolecular organic matter. *Geochim. Cosmochim. Acta* **71**, 4380–4403 (2007).
25. Grimm, E. R. & McSween, Y. H. Heliocentric zoning of the asteroid belt by aluminum-26 heating. *Science* **259**, 653–655 (1993).
26. Piani, L. et al. Origin of hydrogen isotopic variations in chondritic water and organics. *Earth Planet. Sci. Lett.* **567**, 117008 (2021).
27. Alexander, C. M. O. 'D. The origin of inner Solar System water. *Phil. Trans. R. Soc. A* **375**, 20150384 (2017).
28. Floss, C. et al. Identification of isotopically primitive interplanetary dust particles: a NanoSIMS isotopic imaging study. *Geochim. Cosmochim. Acta* **70**, 2371–2399 (2006).
29. McKeegan, K. D. et al. Isotopic compositions of cometary matter returned by Stardust. *Science* **314**, 1724–1728 (2006).
30. Vacher, L. et al. Hydrogen in chondrites: influence of parent body alteration and atmospheric contamination on primordial components. *Geochim. Cosmochim. Acta* **281**, 53–66 (2020).
31. Piani, L. et al. Micron-scale D/H heterogeneity in chondrite matrices: a signature of the pristine solar system water. *Earth Planet. Sci. Lett.* **415**, 154–164 (2015).
32. Lis, D. C. et al. Terrestrial deuterium-to-hydrogen ratio in water in hyperactive comets. *Astron. Astrophys.* **625**, L5 (2019).
33. Piani, L. et al. Earth's water may have been inherited from material similar to enstatite chondrite meteorites. *Science* **369**, 1110–1113 (2020).
34. Salmon, V. et al. Protection of organic matter by mineral matrix in a Cenomanian black shale. *Org. Geochem.* **31**, 463–474 (2000).
35. Tomioka, N. et al. Heating effects of the matrix of experimentally shocked Murchison CM chondrite: comparison to micrometeorites. *Meteorit. Planet. Sci.* **42**, 19–30 (2007).
36. Daly, L. et al. Solar wind contributions to Earth's oceans. *Nat. Astron.* **5**, 1275–1285 (2021).
37. Desch, S. J. et al. The effect of Jupiter's formation on the distribution of refractory elements and inclusions in meteorites. *Astrophys. J. Suppl. Ser.* **238**, 11 (2018).
38. Ito, M. et al. The universal sample holders of microanalytical instruments of FIB, TEM, NanoSIMS, and STXM-NEXAFS for the coordinated analysis of extraterrestrial materials. *Earth Planets Space* **72**, 133 (2020).
39. Uesugi, M. et al. Development of a sample holder for synchrotron radiation-based computed tomography and diffraction analysis of extraterrestrial materials. *Rev. Sci. Instrum* **91**, 035107 (2020).
40. Uesugi, M. et al. Three-dimensional observation of carbonaceous chondrites by Synchrotron radiation X-ray CT–quantitative analysis and developments for the future sample return missions. *Geochim. Cosmochim. Acta* **116**, 17–32 (2013).
41. Greenwood, R. C. et al. Melting and differentiation of early-formed asteroids: the perspective from high precision oxygen isotope studies. *Geochemistry* **77**, 1–43 (2017).
42. Schrader, D. L. et al. A water-ice rich minor body from the early Solar System: the CR chondrite parent asteroid. *Earth Planet. Sci. Lett.* **407**, 48–60 (2014).
43. Starkey, N. A. et al. Triple oxygen isotopic composition of the high $^{3}He/^{4}He$ mantle. *Geochim. Cosmochim. Acta* **176**, 227–238 (2016).
44. Shirai, N. et al. The effects of possible contamination by sample holders on samples to be returned by Hayabusa2. *Meteorit. Planet. Sci.* **55**, 1665–1680 (2020).
45. Ito, M. et al. H, C, and N isotopic compositions of Hayabusa category 3 organic samples. *Earth Planets Space* **66**, 91 (2014).
46. Zolensky, M. E. et al. Mineralogy and composition of matrix and chondrule rims in carbonaceous chondrites. *Geochim. Cosmochim. Acta* **57**, 3123–3148 (1993).
47. Noguchi, T. et al. Variation of mineralogy and organic material during the early stages of aqueous activity recorded in Antarctic micrometeorites. *Geochim. Cosmochim. Acta* **208**, 119–144 (2017).
48. Rowe, W. M. et al. Oxygen isotopes in separated components of CI and CM meteorites. *Geochim. Cosmochim. Acta* **58**, 5341–5347 (1994).
49. Clayton, R. N. & Mayeda, T. K. Oxygen isotope studies of carbonaceous chondrites. *Geochim. Cosmochim. Acta* **63**, 2089–2104 (1999).

Acknowledgements

We thank all of the scientists and engineers of the Hayabusa2 project, whose dedication and skill brought these precious particles back to Earth. The meteorite samples of Orgueil, Y-791198, Y-82162 and Y 980115 were provided by NIPR, Japan. The synchrotron radiation CT experiments were performed at the BL20XU of SPring-8 with the approval of the Japan Synchrotron Radiation Research Institute (JASRI) (grant numbers 2021A0166 and 2021B0188). Synchrotron radiation experiments at SPring-8 are supported by RIKEN. The synchrotron radiation STXM–NEXAFS experiment at BL4U of UVSOR was carried out under the MOU between the JAMSTEC Kochi Institute for Core Sample Research and the Institute for Molecular Science UVSOR synchrotron facility. We thank Marine Works Japan for assistance with sample curation, initial non-destructive investigations and sample preparation of the Ryugu particles. We thank the UK embassy in Tokyo for providing support for the transportation of Ryugu particles from Japan to the United Kingdom. Part of this work was performed at facilities of the Institute for Integrated Radiation and Nuclear Science, Kyoto University. This research was supported in part by the JSPS KAKENHI (grant numbers JP18K18795 and JP18H04468 to M.Ito, JP20H01965 to N.T., JP18H05479 (Innovative Areas 'MFS Materials Science') to M.U., JP19H01959

to A.Y., JP21K03652 to N.I., JP15H05695, JP19H00724 and JP20H01381 to K.U., JP20H00205 to A.T., JP17H06459 to T.U., JP19K03958 to M.Abe, JP17H06459 to T.Okada, JP18K03830 to T.Yada, JP19K23473, JP20K14548 to T.H., JP19K23474 and JP21K13986 to D.Y., JP20K14535 to R.F. and JP17H06459 and JP19H01951 to S.W.), the NIPR Research Project (grant number KP307 to A.Y.) and the Chinese Academy of Sciences President's International Fellowship Initiative (grant number 2019VCA0004 to AT).

Author contributions

M.Ito led the project and wrote the paper with input from all coauthors. M.Ito, N.T., M.U., A.Y., N.S., T.Ohigashi, M-C.L., R.C.G., N.I., Y. Kodama, A.N., K.A.M., N.M., K.D.M. and K.Y. conducted the sample handling, preparation and mounting processes of Ryugu particles. M.Ito, N.T., M.U., T.Ohigashi., K.U., K.H., I.S. and I.O. developed universal sample holders for multiple instruments. M.U., M.Yasutake, A.Tsuchiyama, A.Takeuchi and K.U. arranged and performed SR-CT analysis at SPring-8. SEM–EDS analysis was conducted by A.Y., M.K., N.I. and M.Ito. EPMA analysis and data reduction was conducted by A.Y. XRD analysis was conducted by N.I. FIB sample processing was conducted by Y. Kodama and N.T. STXM–NEXAFS analysis was conducted by T.Ohigashi, H.Y., M.I., M.U and A.N. NanoSIMS analysis was conducted by M.Ito. TEM work was done by N.T. Oxygen isotopes were measured by R.C.G., R.F., I.A.F. and J.A.M at the Open University. N.S. and S.Sekimoto conducted INAA analysis at Kyoto University. M.Arakawa, A.F., M.F., M.H., Naoyuki Hirata, Naru Hirata, R.H., C.H., S.H., Y.Iijima, H.I., M.Ishiguro, Y.Ishihara, T.I., K.Kawahara, S.K., K.Kitazato, K.M., M.M., T.Michikami, Y.Mimasu, A.Miura, O.M., T.Morota, S.N., N.N., H.N., R.N., N.O., K.O., T.Okada., C.O., G.O., M.O., T.S., N.S., H.Sawada, H.Senshu, Y.S., K.S., S.Sugita, Y.Takei, H.T., S.T., E.T., F.T., R.T., K.W., M.Yamada, T.Y., Y.Yamamoto, H.Y., Y.Yokota, K.Y., M.Yoshikawa and K.Yoshikawa. S.W. and Y.Tsuda contributed to the spacecraft operations and selected sampling sites. R.F., S.F., K.H., T.H., Y.H., K.Kumagai, A.M., M.N., H.Hitomi, A.I., D.Y., M.Yoshitake, T.Yada, M.Abe and T.U. led the JAXA curation activities for the initial characterization of allocated Ryugu particles. M.Yoshikawa, T.S., S.T., F.T., S.N., S.Sugita, K.Kitazato, T.Okada, Naru Hirata, S.W. and Y. Tsuda administered the project and acted as principal investigators. All authors contributed to the data interpretation, commented and finalized the paper.

Competing interests

The authors declare no competing interests.

Additional information

Extended data is available for this paper at https://doi.org/10.1038/s41550-022-01745-5.

Supplementary information The online version contains supplementary material available at https://doi.org/10.1038/s41550-022-01745-5.

Correspondence and requests for materials should be addressed to Motoo Ito.

Peer review information *Nature Astronomy* thanks Ashley King, Jemma Davidson and the other, anonymous, reviewer(s) for their contribution to the peer review of this work.

Reprints and permissions information is available at www.nature.com/reprints.

Publisher's note Springer Nature remains neutral with regard to jurisdictional claims in published maps and institutional affiliations.

[1]Kochi Institute for Core Sample Research, X-Star, Japan Agency for Marine-Earth Science Technology (JAMSTEC), Nankoku, Japan. [2]Japan Synchrotron Radiation Research Institute (JASRI/SPring-8), Sayo, Japan. [3]National Institute of Polar Research (NIPR), Tokyo, Japan. [4]The Graduate University for Advanced Studies (SOKENDAI), Hayama, Japan. [5]Graduate School of Science, Department of Chemistry, Tokyo Metropolitan University, Tokyo, Japan. [6]UVSOR Synchrotron Facility, Institute for Molecular Science, Okazaki, Japan. [7]Department of Earth, Planetary, and Space Sciences, UCLA, Los Angeles, CA, USA. [8]The Open University, Milton Keynes, UK. [9]Institute of Space and Astronautical Science (ISAS), Japan Aerospace Exploration Agency (JAXA), Sagamihara, Japan. [10]Marine Works Japan, Ltd, Yokosuka, Japan. [11]Research Organization of Science and Technology, Ritsumeikan University, Shiga, Japan. [12]CAS Key Laboratory of Mineralogy and Metallogeny/Guangdong Provincial Key Laboratory of Mineral Physics and Materials, Guangzhou Institute of Geochemistry, Chinese Academy of Sciences (CAS), Guangzhou, China. [13]CAS Center for Excellence in Deep Earth Science, Guangzhou, China. [14]Department of Mechanical Engineering, Osaka University, Osaka, Japan. [15]Institute for Integrated Radiation and Nuclear Science, Kyoto University, Osaka, Japan. [16]Synchrotron Radiation Research Center, Nagoya University, Nagoya, Japan. [17]JAXA Space Exploration Center, JAXA, Sagamihara, Japan. [18]Kobe University, Kobe, Japan. [19]University of Aizu, Aizu-Wakamatsu, Japan. [20]Kochi University, Kochi, Japan. [21]Department of Physics and Astronomy, Seoul National University, Seoul, Republic of Korea. [22]Chiba Institute of Technology, Narashino, Japan. [23]National Astronomical Observatory of Japan, Mitaka, Japan. [24]Kindai University, Higashi-Hiroshima, Japan. [25]The University of Tokyo, Tokyo, Japan. [26]Niigata University, Niigata, Japan. [27]Rikkyo University, Tokyo, Japan. [28]Instituto de Astrofísica de Canarias, University of La Laguna, Tenerife, Spain. [29]Kanagawa Institute of Technology, Atsugi, Japan. [30]Earth-Life Science Institute, Tokyo Institute of Technology, Tokyo, Japan. [31]Nagoya University, Nagoya, Japan. [32]Present address: Department of Chemistry, Faculty of Science, Kanagawa University, Yokohama, Japan. [33]Present address: Photon Factory, Institute of Materials Structure Science, High Energy Accelerator Research Organization, Tsukuba, Japan. [34]Present address: Toyo Corporation, Tokyo, Japan. [35]Present address: Center for Data Science, Ehime University, Matsuyama, Japan. [36]Present address: Toyo University, Tokyo, Japan. [37]Present address: Japan Patent Office, Tokyo, Japan. [38]Deceased: Yu-ichi Iijima, Chisato Okamoto. ✉e-mail: motoo@jamstec.go.jp

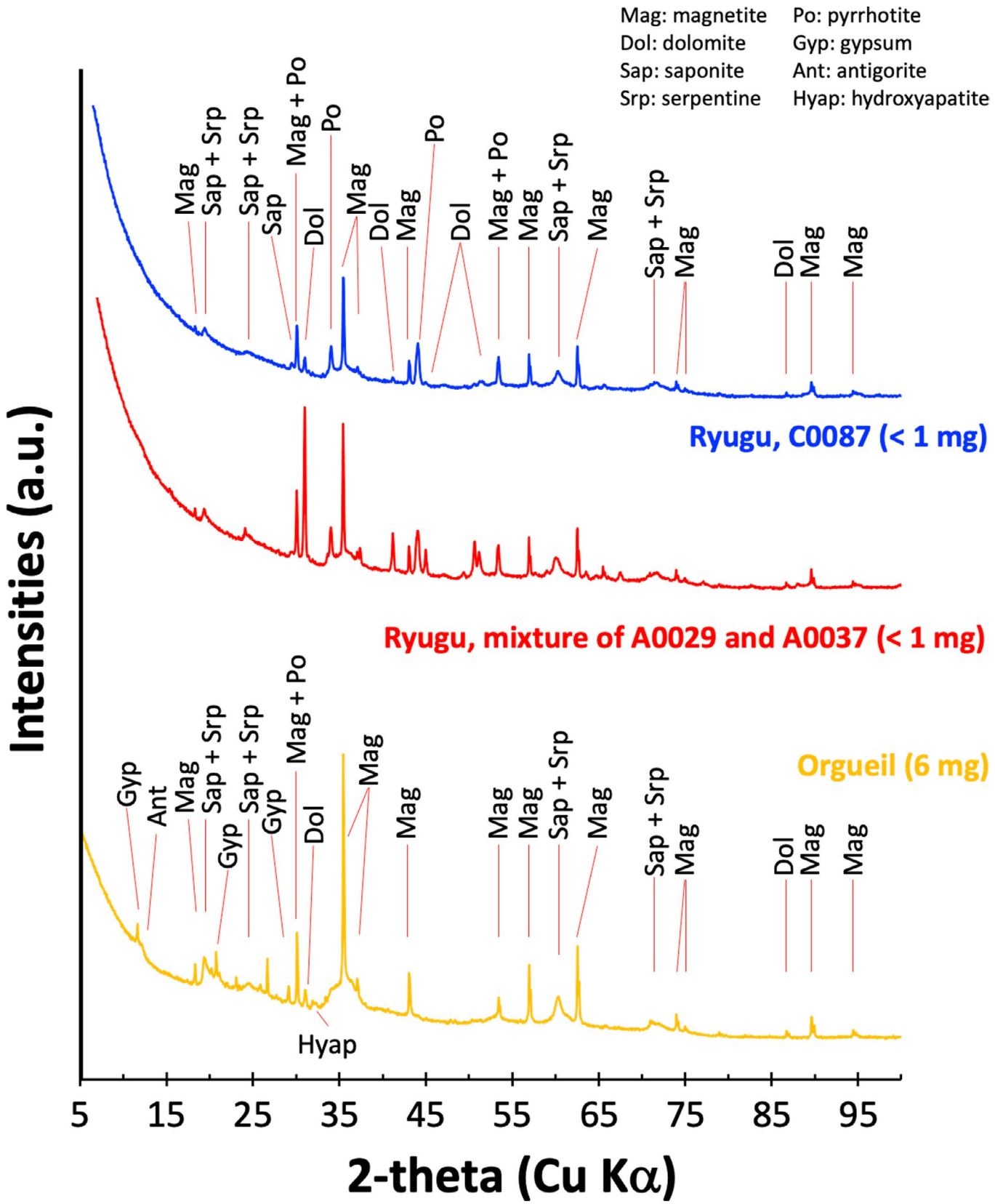

Extended Data Fig. 1 | Powder XRD patterns of Ryugu C0087 (blue line), a mixture of A0029 and A0037 (red line) in comparison with a CI chondrite Orgueil (orange line). The dolomite peak for the Chamber A particles (mixture of A0029 and A0037) is much more intense than that for the Chamber C particle (C0087), which is consistent with the estimated abundance from the polished sections (see Supplementary Data 1).

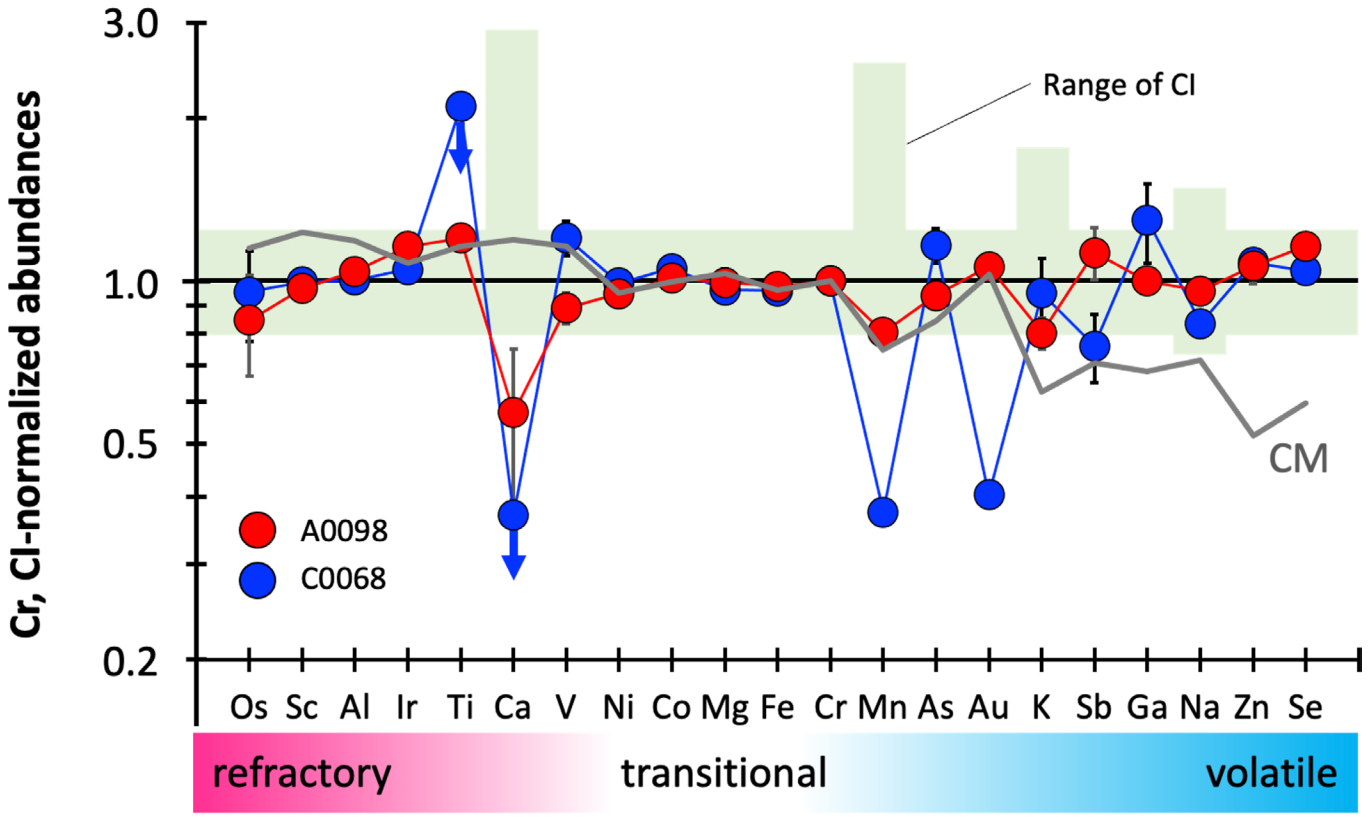

Extended Data Fig. 2 | Bulk chemical abundances of Ryugu particles. A0098 (1.6303 mg, filled red circles) and C0068 (0.6483 mg, filled blue circles) are compared with the composition of CI (shaded green area) and CM (grey line) chondrites. The elements are ordered by each volatility.